Ultralow-Density Nanocage-Based Metal-Oxide Polymorphs

Javier Carrasco,[1] Francesc Illas,[1] and Stefan T. Bromley[1,2,*]

[1]*Dept. Química Física & IQTCUB, Universitat de Barcelona, 08028 Barcelona, Spain*
[2]*Institució Catalana de Recerca i Estudis Avançats (ICREA), 08010 Barcelona, Spain*

(Received 7 June 2007; published 4 December 2007)

For two important metal oxides (MO, M=Mg, Zn) we predict, via accurate electronic structure calculations, that new low-density nanoporous crystalline phases may be accessible via the coalescence of nanocluster building blocks. Specifically, we consider the assembly of cagelike $(MO)_{12}$ clusters exhibiting particularly high gas phase stability, leading to new polymorphs with energetic stabilities rivaling (and sometimes higher) than those of known MO polymorphs.

DOI: 10.1103/PhysRevLett.99.235502 PACS numbers: 61.43.Gt, 61.46.Bc, 71.15.Nc, 82.75.Fq

Exhibiting a cubic crystal structure in its bulk equilibrium phase at ambient conditions, rock salt magnesium oxide (rs-MgO) is a prototypical example of a stable, densely packed insulating ionic system. Bulk ZnO may be stabilized in a cubic rock salt phase (rs-ZnO) under high pressure [1] but prefers to adopt a wurtzite ground state structure (wz-ZnO) under ambient conditions. ZnO is also a wide band gap semiconductor with (nano)technological potential in numerous applications (e.g., optoelectronics, sensors). Theoretical studies have examined numerous bulk polymorphs of MgO and ZnO [2,3] focusing mainly on known dense crystal phases exhibited in other materials. Under conditions of high temperatures [4] and/or reduced dimensionality (e.g., thin films [5]) studies have further reported strong evidence for alternative phases of MgO. At the nanoscale, recent interest in the properties of ZnO has been intense with theoretical predictions of hexagonal phases for various reconstructed [6,7] and strained nanostructures [8]. In all cases, the reported bulk or nanoscale phases are denser than the wz-ZnO phase for ZnO, and for MgO have maximum volumes per unit cell of up to ~30% greater than rs-MgO. Our approach, considering clusters as building blocks [9], bypasses the constraint of considering known dense phases as sources of new polymorphs (e.g., via pressure-induced transformations), showing that it should be possible to stabilize new nanoporous polymorphic phases of both ZnO, with unit cell volumes between 20–70% greater than wz-ZnO, and MgO, with unit cell volumes 50–110% greater than rs-MgO. To our knowledge the polymorphs we propose have not been reported for any other MO material but have strong topological links with certain SiO_2-based nanoporous crystals. Following the formation of silicate-based zeolitic phases we have attempted to assess the viability of our proposed polymorphs via nanoscale bottom-up routes using $(MO)_{12}$ cage clusters as building blocks via calculating (i) the thermodynamic and kinetic stability of $(MO)_{12}$ cages with respect to competing isomers and (ii) the energetics of cage-cage interactions. Via determining the equation of state (EOS) for each of our MO polymorphs, we find three phases with energies 0.15–0.27 eV/MO above their respective ambient ground states. Considering that the synthesized rs-ZnO polymorph lies 0.29 eV/ZnO above wz-ZnO these polymorphs seem attractive synthesis targets. Further, all our polymorphs have the lowest reported energies (at their respective densities) of any reported MgO/ZnO polymorph and are thus potential thermodynamically favored equilibrium states for MgO and ZnO for conditions allowing for low density phases.

Energies, structures, and electronic states of cluster isomers and bulk phases of MgO and ZnO were calculated using inherently size transferable density functional theory (DFT) using the PW91 exchange-correlation potential [10] and the projector-augmented-wave method [11] with a 415 eV energy cutoff for valence states. Monkhorst-Pack grids of k points: rs-MgO(ZnO): $7\times7\times7(11\times11\times11)$, wz-MgO(ZnO): $5\times5\times5(7\times7\times7)$, h-MgO(ZnO): $5\times5\times5(11\times11\times11)$, SOD-MgO(ZnO): $7\times7\times7(9\times9\times9)$, Linde Type A (LTA) MgO(ZnO): $3\times3\times3(5\times5\times5)$, Faujasite (FAU) MgO(ZnO): $2\times2\times2(3\times3\times3)$ and $1\times1\times1$ for isolated clusters were used (where the naming notation is explained below). For bulk phases the volume versus energy data was fitted using the Birch-Murnaghan EOS [12]. To generate low energy isomers of $(MO)_{12}$ we used the basin-hopping global optimization method [13] with Born interatomic potentials following studies on MgO [14] and ZnO [15] clusters. To effectively represent the range of $(MO)_{12}$ structural preferences due to ionic polarization, the $M^{q+}O^{q-}$ charges were varied between 1 and 1.5, at intervals of 0.1, performing global optimizations for each q. Cluster isomer energies and structures were refined using DFT energy minimizations. Transition state structures between cluster minima of interest were located by the climbing image nudged elastic band algorithm [16], where transition path stability was verified by manual perturbation of the initial path geometries. Stationary states were characterized by harmonic vibrational frequency analysis showing that all minima have all positive frequencies and transition states one negative frequency. The VASP code was used throughout [17].

Cluster beam studies of $(MgO)_N$ clusters give mass spectra with high relative abundance peaks observed at

specific "magic" numbers for $(MgO)_{3n}$ ($n = 2$–6, 8–10) [18,19], indicating that these sizes correspond to isomers of exceptional stability. Although these compositions are consistent with a set of increasingly sized $(3 \times 2)_n$ cubic slab geometries reminiscent of rs-MgO, efforts to assign structures to these peaks using classical interionic potentials have met with mixed success due to the high dependency of cluster structure on the atomic charge distribution [14,19]. Our DFT-refined global optimization predictions are largely in agreement with the most transferable classical investigations [20] and with studies employing cluster-based electronic structure methods [21–23], although we also find some new isomers (see Fig. 1). For small $(MgO)_{3n}$ ($n = 2$–5) clusters we predict hexagonal tubelike nanoclusters are energetically favored, with cubic isomers ~0.05–0.07 eV/MgO higher in energy. For $(MgO)_{12}$ the tubelike ground state is almost energetically degenerate with a highly symmetric cage isomer having an excess energy of only ~0.015 eV/MgO. In experiment, the existence of clusters nearly degenerate with the ground state allows for a mix of isomers to contribute to a single mass resolved peak. Further, due to the differences in experimental conditions and in techniques employed to generate clusters (e.g., bulk fragmentation, monomer nucleation), and in the nature of the free energy landscape, the most abundant isomer may be not the lowest energy isomer but a competing isomer that is kinetically trapped by a significant energy barrier from reaching the global energetic ground state [24]. We have calculated the energy barriers for the transitions between the three lowest energy $(MgO)_{12}$ isomers (see Fig. 2) with initial and final state atom mappings based on topological similarities. The transition between a $(MgO)_{12}$ cubic slab and hexagonal tube presents a very small barrier (~0.09 eV). The $(MgO)_{12}$ cage-to-tube and tube-to-cage transitions proceed via the very weak minima of isomer $(MgO)_{12}$-f (see Fig. 1) and both have an overall high barrier (>0.8 eV) showing the strong metastability of the $(MgO)_{12}$ cage isomer with respect to the marginally lower energy tube isomer and, depending on experimental conditions, could persist indefinitely. In experiments cluster populations are often ionized to facilitate control and avoid aggregation, which may lead to isomer selection via ease of ionization rather than only neutral energetic stability. We stress that this would be an experimentally dependent post-selection process on an existing abundant neutral $(MgO)_{12}$ isomer population. Based upon our analysis, although cubic $(MgO)_{12}$ clusters would be very unlikely in preionized isomer populations, it is feasible that the resulting observed magic peak for $(MgO)^+_{12}$ clusters results from an ensemble of neutral tube and cage isomers.

We are unaware of any cluster beam experiments for $(ZnO)_N$, $N \leq 12$ and the energetically low lying isomer spectrum in this size range must be determined solely by theory. Most theoretical studies of ZnO clusters have used electronic structure methods to establish likely $(ZnO)_N$ ground states with the cage isomer given as the most stable cluster for $(ZnO)_{12}$ [15,25]. Our DFT-refined global optimization calculations concur with this result but further find that the second highest energy isomer is a hitherto unreported distorted cagelike cluster lying 0.11 eV/ZnO above the ground state (see Fig. 1). Unlike $(MgO)_{12}$, which possesses competing isomers in this energy range, this relatively large separation signifies that if $(ZnO)_{12}$ clusters were to be isolated in gas phase then the cage isomer would likely be the dominant species in the isomer population. Comparing the relative energetic stability of $(ZnO)_{12}$ with cluster isomers possessing greater or fewer ZnO units also provides predictive measures of likely isomer abundances in a cluster population. Such stability measures are found to be peaked at $n = 12$ [15,25], indicating that $(ZnO)_{12}$, like $(MgO)_{12}$, is a magic cluster size indicating that the $(ZnO)_{12}$ cage would be conspicuously abundant in cluster beams.

If magic cagelike $(MO)_{12}$ isomers (M = Zn, Mg) were isolated in significant quantities, it is reasonable to assume

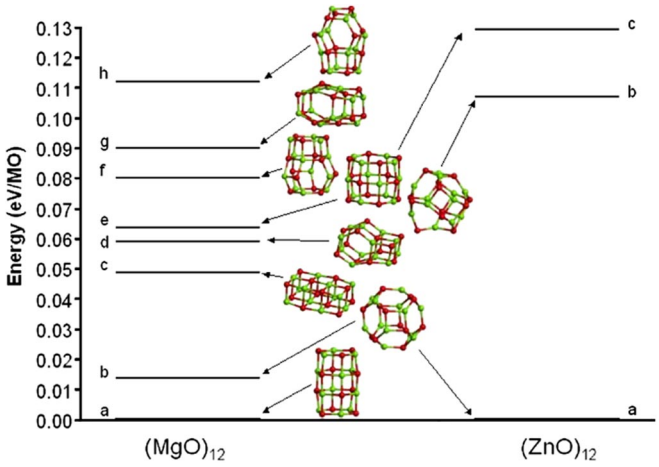

FIG. 1 (color online). Low energy isomer spectrum of $(MgO)_{12}$ and $(ZnO)_{12}$.

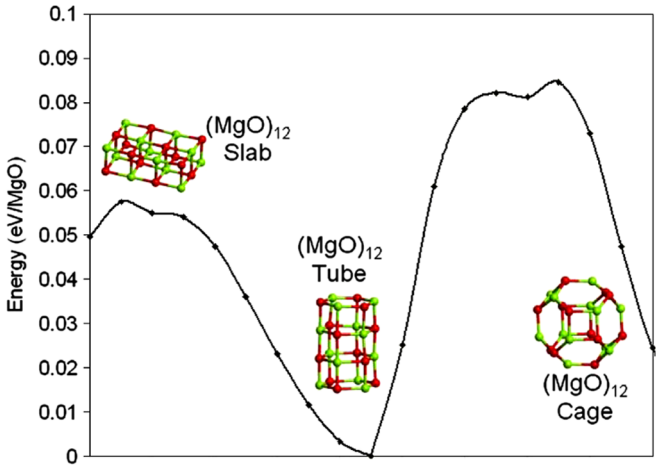

FIG. 2 (color online). Energetics for transitions between tube, cage, and slab $(MgO)_{12}$ isomers.

that they could act as building blocks to form higher order structures (e.g., via deposition on a substrate or gas phase nucleation). Unlike magic metal clusters, which tend to lose their discrete structural identity when coalescing [26], the rigid faceted $(MO)_{12}$ cages may link together in a more orderly fashion while retaining their open structure. The $(MO)_{12}$ cage presents two different faces [square $(MO)_{12}$, hexagonal $(MO)_6$] and two types of edge (linear M-O). Bringing two cages together in either a face-to-face or edge-to-edge manner we have found that the coalescence of two $(MO)_{12}$ cages is barrierless and energetically favorable and results in structurally stable products. Considering that the topology of the 24 atoms of a $(MO)_{12}$ cage is analogous to that of silicon atoms in the so-called sodalite (SOD) cage exhibited in numerous silicate zeolite crystals [27], we may imagine a continuation of this aggregation process to form zeoliticlike nanoporous bulk MO phases. In this way we have constructed three new crystalline nanoporous X-MO phases (X = FAU, LTA, or SOD, following the framework notation for the corresponding silicate topologies [27]); see Fig. 3. In each case, the X-MO phase is constituted solely by the bonded assembly of $(MO)_{12}$ cages: (i) FAU-MO by bonding via $(MO)_6$ hexagonal faces forming intercluster hexagonal prisms, (ii) LTA-MO by $(MO)_2$ square-square interfacial bonding, forming cubic cluster-cluster linkages, and (iii) SOD-MO via M-O edge-to-edge intercage interactions forming square $(MO)_2$ linkages. For each nanoporous zeolitic MO framework, together with rs-MO, a hexagonal polymorph h-MO [4,7,28], and the wz-MO phase, we calculate total energy versus volume EOS for both MgO and ZnO, respectively (Fig. 4). From these fits the equilibrium values of the volume (V_0), the total energy (E_0), and the isothermal bulk modulus (B_0) of all phases were obtained and summarized, together with the relative band gap magnitudes, in the insets of Fig. 4. As is usual for DFT calculations, the absolute band gaps are systematically underestimated (i.e., rs-MgO: 4.55 eV, wz-ZnO: 0.76 eV) whereas the relative magnitudes provide an internal gauge of the electronic change with respect to change in bulk topology.

The MgO nanoporous phase minima are lower in energy than all extrapolated curves corresponding to the EOS of any previously reported phase. The new polymorphs are also stable under compression and expansion with respect to the previously proposed wz-MgO [4] and h-MgO [28] phases and with respect to each other. Conversions between the cage $(MgO)_{12}$ cluster and other isomers are hindered by large energy barriers. It thus seems unlikely that these new phases would be easily accessed via negative-pressure and/or high temperature treatments applied to the rs-MgO or h-MgO phases. The energy above rs-MgO increases with increasing volume per MgO unit: SOD-MgO: 0.28 eV/MgO, LTA-MgO: 0.44 eV/MgO, FAU-MgO: 0.49 eV/MgO, where the volume/MgO is, respectively, 55%, 90%, and 114% larger than that of rs-MgO. In the new phases the Mg and O atoms are tetrahe-

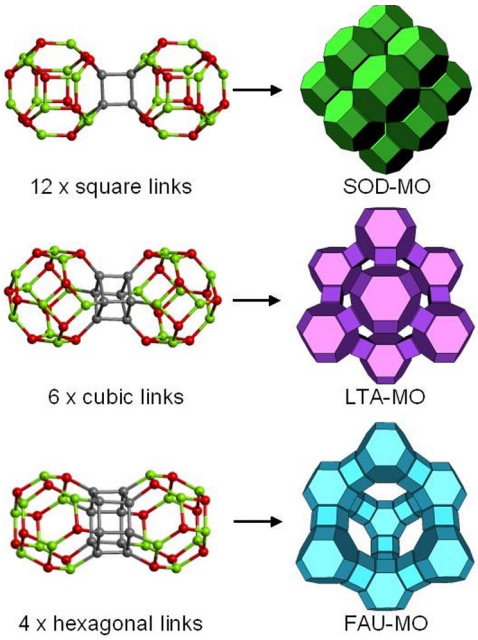

FIG. 3 (color online). Schematic showing $(MO)_{12}$ nanocage assembly of zeolitic MO phases.

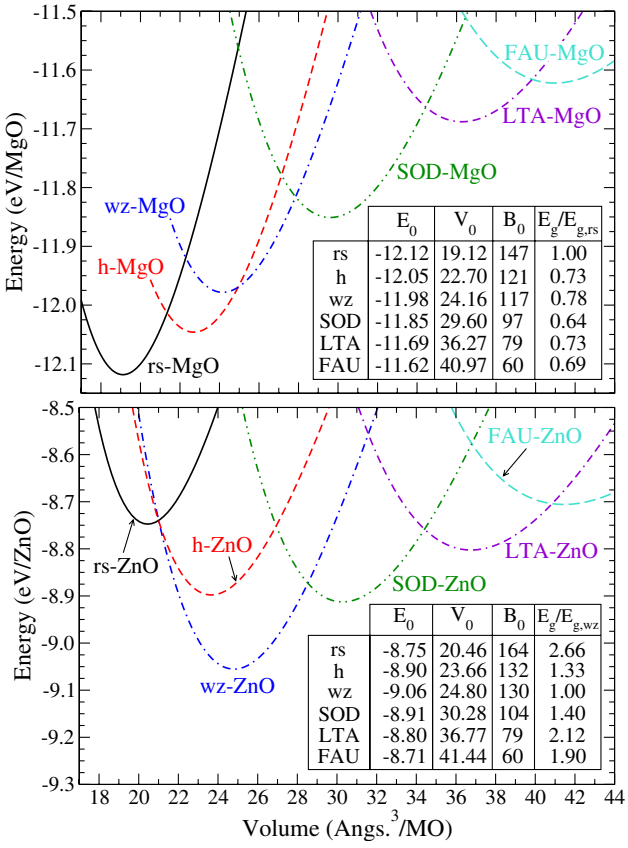

FIG. 4 (color online). Equation of state for MO polymorphs. Insets give equilibrium values of total energy per MO unit (E_0), volume per MO unit (V_0, Å^3), band gap relative to ground state MO phase, and the bulk modulus (B_0, GPa).

drally coordinated centers, unlike their sixfold-coordinated environment in rs-MgO, allowing for lower densities and leading to polymorphs with higher flexibility and/or compressibility (lower bulk moduli with respect to rs-MgO) and smaller electronic band gaps; see Fig. 4. There is no simple correspondence between structure and/or density and band gap with both the dense sixfold-coordinated *h*-MgO phase and the low-density fourfold-coordinated LTA-MgO polymorph having the same gap. The smallest gap is found for the lowest energy nanoporous polymorph SOD-MgO, being 36% lower than for the rs-MgO phase.

The ZnO nanoporous polymorphs follow the order of decreasing density and bulk modulus as the respective MgO phases but have a different order of energetic stability. The synthesized high-pressure rs-ZnO cubic phase lies 0.29 eV/ZnO above wz-ZnO. Three polymorphs, SOD-ZnO, *h*-ZnO, and LTA-ZnO, are found to be lower in energy than rs-ZnO. Although it is perhaps expected that the *h*-ZnO phase, having density between that of rs-ZnO and wz-ZnO, should also lie within the corresponding energy range, the stability of the SOD-ZnO and LTA-ZnO phases being 18% and 40% less dense, respectively, than wz-ZnO is more surprising. Our calculations suggest that the SOD-ZnO phase is marginally more stable than the *h*-ZnO phase and lies 0.15 eV/ZnO above wz-ZnO, making it a particularly promising synthetic target. The band gaps of the new ZnO phases are all higher than for wz-ZnO but due to their open nanoporous framework structures, if synthesized, present opportunities for doping (e.g., via metal atoms and/or clusters) as a means to tailor their electronic structure.

Using accurate theoretical methods consistently at the nanoscale and in the bulk we show that important necessary conditions for viable nanofabrication of novel ultralow-density crystalline nanoporous polymorphs of MgO and ZnO are fulfilled: (i) existence of very low energy kinetically stable nanocage clusters, (ii) energetically favorable and structurally stable intercluster interactions allowing bulk formation via cluster nucleation, and (iii) energetic/structural stability of final MO nanoporous bulk phases with respect to other polymorphs. Considering typical excess energies with respect to the ambient ground state of synthesized amorphous oxide phases (e.g., amorphous ZrO_2: 0.35 ± 0.04 eV/ZrO_2 [29]) together with typical energetic criteria for the feasibility of hypothetical nanoporous silicate frameworks (<0.31 eV/SiO_2 [30]), the energetic expense of forming these new low-density nanoporous oxides does not seem prohibitive. The (nano)-technological value of nanoporous oxides is undoubted with the widespread use of SiO_2-based zeolites. We show that analogous nanoporous phases are viable in other oxides, offering a wider range of electronic, chemical, and structural possibilities and hope that this study will stimulate experimental efforts toward the synthesis of these novel materials.

We acknowledge Projects No. CTQ2005-08459-CO2-01, No. UNBA05-33-001, No. 2005SGR-00697, and No. 2005 PEIR 0051/69, and computer time on MareNostrum (Barcelona Supercomputing Center).

*Corresponding author

[1] S. Desgreniers, Phys. Rev. B **58**, 14102 (1998).
[2] A. Schleife, F. Fuchs, J. Furthmüller, and F. Bechstedt, Phys. Rev. B **73**, 245212 (2006).
[3] J. C. Schon, Z. Anorg. Allg. Chem. **630**, 2354 (2004).
[4] A. Aguado and P. A. Madden, Phys. Rev. Lett. **94**, 068501 (2005).
[5] J. Goniakowski, C. Noguera, and L. Giordano, Phys. Rev. Lett. **93**, 215702 (2004).
[6] C. L. Freeman, F. Claeyssens, N. L. Allan, and J. H. Harding, Phys. Rev. Lett. **96**, 066102 (2006).
[7] L. Zhang and H. Huang, Appl. Phys. Lett. **90**, 023115 (2007).
[8] A. J. Kulkarni, M. Zhou, K. Sarasamak, and S. Limpijumnong, Phys. Rev. Lett. **97**, 105502 (2006).
[9] J. C. Wojdel, M. A. Zwijnenburg, and S. T. Bromley, Chem. Mater. **18**, 1464 (2006).
[10] J. P. Perdew, J. A. Chevary, S. H. Vosko, K. A. Jackson, M. R. Pederson, D. J. Singh, and C. Fiolhais, Phys. Rev. B **46**, 6671 (1992); J. A. White and D. M. Bird, Phys. Rev. B **50**, 4954 (1994).
[11] G. Kresse and D. Joubert, Phys. Rev. B **59**, 1758 (1999).
[12] F. Birch, Phys. Rev. **71**, 809 (1947).
[13] D. J. Wales and J. P. K. Doye, J. Phys. Chem. A **101**, 5111 (1997).
[14] C. Roberts and R. L. Johnston, Phys. Chem. Chem. Phys. **3**, 5024 (2001).
[15] B. Wang, S. Nagase, J. Zhao, and G. Wang, J. Phys. Chem. C **111**, 4956 (2007).
[16] G. Henkelman and H. Jonsson, J. Chem. Phys. **113**, 9978 (2000).
[17] G. Kresse and J. Hafner, Phys. Rev. B **47**, 558 (1993).
[18] P. J. Ziemann and A. W. Castleman, Jr., J. Chem. Phys. **94**, 718 (1991).
[19] W. A. Saunders, Phys. Rev. B **37**, 6583 (1988).
[20] M. Wilson, J. Phys. Chem. B **101**, 4917 (1997).
[21] J. M. Recio, R. Pandey, A. Ayuela, and A. B. Kunz, J. Chem. Phys. **98**, 4783 (1993).
[22] A. Aguado and J. M. López, J. Phys. Chem. B **104**, 8398 (2000).
[23] F. Bawa and I. Panas, Phys. Chem. Chem. Phys. **4**, 103 (2002).
[24] F. Baletto, A. Rapallo, G. Rossi, and R. Ferrando, Phys. Rev. B **69**, 235421 (2004).
[25] A. C. Reber, S. N. Khanna, J. S. Hunjan, and M. R. Beltran, Eur. Phys. J. D **43**, 221 (2007).
[26] H. Häkkinen and M. Manninen, Phys. Rev. Lett. **76**, 1599 (1996).
[27] *Handbook of Zeolite Science and Technology*, edited by S. A. Auerbach *et al.* (Marcel Dekker, Inc., New York, 2003).
[28] S. Limpijumnong and W. R. L. Lambrecht, Phys. Rev. B **63**, 104103 (2001).
[29] A. Navrotsky, Proc. Natl. Acad. Sci. U.S.A. **101**, 12 096 (2004).
[30] M. D. Foster *et al.*, Nature Mater. **3**, 234 (2004).